Optics Communications 549 (2023) 129834

Contents lists available at ScienceDirect

Optics Communications

journal homepage: www.elsevier.com/locate/optcom

Tailoring the bound states in the multi-channel nonlinear plasmonic metasurfaces

Xiuyu Wang [a,1], Xiaoman Wang [a,1], Jihong Xin [a,1], Jitao Li [c], Qun Ren [b], Haocheng Cai [b,*], Yuxin Lang [b], Zhihao Lan [d], Yuqi Jia [b], Ruiqi Jin [b], Yuqing He [b], Jian Wei You [e], Wei E.I. Sha [f], Yanwei Pang [b]

[a] Tianjin Key Laboratory of Imaging and Sensing Microelectronic Technology, School of Microelectronics, Tianjin University, Tianjin 300072, China
[b] School of Electrical and Information Engineering, Tianjin University, Tianjin 300072, China
[c] School of Precision Instrument and Opto-electronics Engineering, Tianjin University, Tianjin 300072, China
[d] Department of Electronic and Electrical Engineering, University College London, London WC1E7JE, UK
[e] State Key Laboratory of Millimeter Waves, School of Information Science and Engineering, Southeast University, Nanjing 210096, China
[f] Key Laboratory of Micro-Nano Electronic Devices and Smart Systems of Zhejiang Province, College of Information Science and Electronic Engineering, Zhejiang University, Hangzhou 310027, China

ARTICLE INFO

Keywords:
Bound states in the continuum
Nonlinear metasurfaces
Second harmonic generation efficiency

ABSTRACT

Metasurfaces offer a paradigm shift in the nonlinear optics, controlling and enhancing of nonlinear effects at the nanoscale, and offering new opportunities for applications in nonlinear optics, plasmonics and electromagnetics. Particularly, nonlinear optical conversion efficiency is limited due to the inherent losses in metallic materials. Nonlinear metasurfaces based on bound states in the continuum(BIC) can effectively increase the Q value and are expected to further enhance the nonlinear efficiency. In this paper, a tri-capacitance-like metasurface supporting both Friedrich–Wintgen quasi-BIC and symmetry-protected quasi-BIC is proposed to generates multiple high-Q resonances in the spectrum. The coupling between perfect BIC and quasi-BIC mode in the multi-channel optical system corresponds to the storage and release of electromagnetic waves, respectively. At the same time, the electromagnetic field is further enhanced at the resonant frequency, which can significantly improve the second order nonlinear efficiency. In addition, due to the different generation mechanism, the frequency and amplitude of the two resonances are easy to tune independently, which facilitates the sum and difference frequency generation (SFG and DFG). Therefore, the proposed nonlinear metasurfaces in this paper are of wide research value in the fields of nonlinear optics, multi-channel communication and memory.

1. Introduction

As an alternative of conventional optical devices, metamaterials, which consist of periodic subwavelength metallic/dielectric structures that resonantly couple to either or both components of the incident electromagnetic field [1], exhibit an effective electromagnetic response which is not found in materials in nature [2,3], meeting the requirements for integration and miniaturization in modern electromagnetic and photonic systems [4]. The electromagnetic properties of metamaterials are mainly determined by the structural geometry and the integrated material [5,6], and by designing artificial unitary structures capable of producing the desired electromagnetic response and device functionality [7,8]. However, the development of metamaterials for practical applications is impeded by the fact that the permittivity, permeability and refractive index are properties of three-dimensional objects, while three-dimensional microscopic nanostructures still present difficulties in fabrication [9]. As manufacturing technology continue to develop, two-dimensional planar materials can be fabricated by means of photolithography and nano-printing [10,11], and researchers have begun to investigate metamaterials with single or multiple layers stacked on top of each other. These metamaterials are called metasurfaces, two-dimensional equivalents of three-dimensional metamaterials [12,13]. In optical systems, the design of structure and the period of the sub-wavelength unit cell of the metasurfaces enables

* Corresponding author.
E-mail addresses: renqun@tju.edu.cn (Q. Ren), caihc1990@163.com (H. Cai), pyw@tju.edu.cn (Y. Pang).
[1] These authors contributed equally to this work.

https://doi.org/10.1016/j.optcom.2023.129834
Received 20 February 2023; Received in revised form 29 July 2023; Accepted 13 August 2023
Available online 16 August 2023

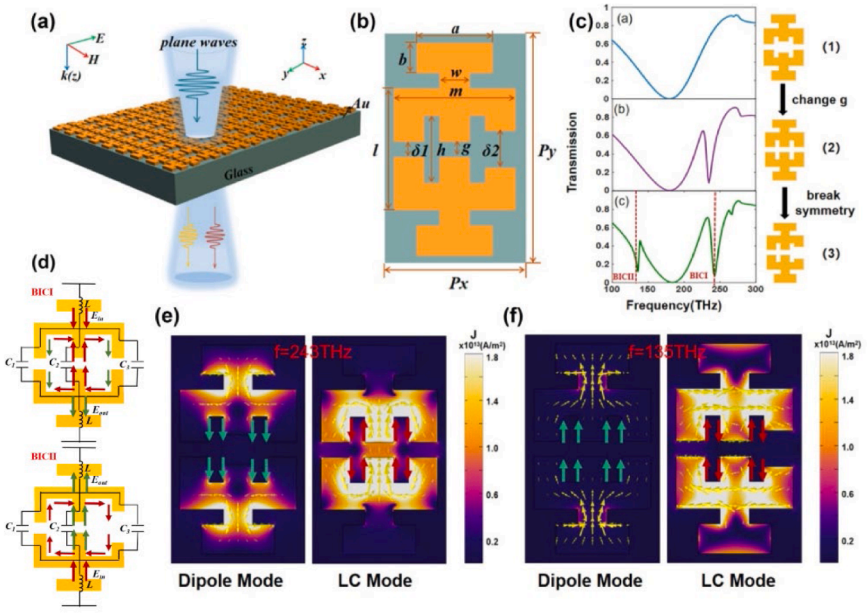

Fig. 1. (a) The schematic view of proposed tri-capacitance-like metasurface. (b) The unit cell of the metasurface. (c) Transmission spectra for g = 100 nm, $\delta 1 = \delta 2 =$ 50 nm (1), g = $\delta 1 = \delta 2 =$ 50 nm (2) and g = $\delta 1 =$ 50 nm, $\delta 2 =$ 120 nm (3). (d) The corresponding circuit model of metasurface. (e) and (f) show the current distribution at frequency of BICI and BICII respectively.

wavefront modulation of the optical field [12,14,15], anomalous reflection [16] and transmission [17] as well as local field enhancement [13], overcoming the development challenges of metamaterials in practical applications.

Nonlinear metasurfaces, with the independent development of plasmonics and nano-devices [18], is a frontier in the field of metamaterials [19,20]. Due to the ability of metasurfaces to convert incident light into harmonics with anomalous polarization, nonlinear metasurfaces is also spotlighted and expected to further advance nonlinear optics, achieving a robust nonlinear optical response in a more compact size, and relaxing or completely overcoming the phase matching requirement [21]. Typically, the quality factor(Q) of nonlinear metasurfaces is very low due to the inherent loss of metallic metasurfaces, and their nonlinear conversion efficiency is very limited [22–24]. The perfect bound states in the continuum(BIC) [25] with a theoretically infinite Q value [26,27] would excite a greatly enhanced resonance mode, which will likely lead to a fundamental breakthrough in optical nonlinear efficiency [28]. BICs can be divided into two types, symmetry-protected BICs [29–31], which arises from symmetry incompatibility between bound states and external fields, and asymmetry-protected BICs (called as accidental BICs), which arises from destructive interference between the leaking channels of the system [25,32]. Accidental BICs can be further classified into three cases, Fabry–Perot BIC [33], Friedrich–Wintgen BIC [32] and single-resonance parametric BIC [34].

Based on BIC, the design of the nonlinear metasurfaces unit cell structure can also achieve electromagnetic filtering [35], super-resolution [36–38] and optical modulation functions [39,40], which further needs high-capacity optical channels in a compact device. Specifically, the mutual coupling between multiple optical resonances is expected to enable multi-channel communication and applications of SFG and DFG [41,42]. In addition, the different modes in the optical resonance coupling process accompany different surface current distributions, which macroscopically manifest as the storage and release of electromagnetic waves that is a promising technology that can motivate the realization of optical memories and quantum memories [43–48].

On the basis of the above research background, this paper proposes a tri-capacitance-like metallic metasurface with high Q, multi-channel resonance and electromagnetic wave storage and release. Firstly, the Friedrich–Wintgen quasi-BIC is excited without breaking the structural symmetry by adjusting the structural parameters to obtain a high-Q resonance. Later, a symmetry-protected quasi-BIC is excited by breaking the structural symmetry to achieve a two-channel optical resonance. The frequency and amplitude of the resonances can be adjusted by changing the structural parameters and are adjustable with a high degree freedom due to the different generation mechanism. Secondly, at the resonant frequency, the current distribution on the metasurface is also different, corresponding to the storage and release of electromagnetic waves, respectively. Finally, the electromagnetic field distribution at the resonant frequency is simulated, and the study shows that the metasurface structure designed in this paper can effectively enhance the second-order nonlinear effect. The results show that the metasurface we proposed have significant research value in second harmonic generation (SHG), SFG, DFG, multi-channel communication and memory.

2. Design and structure

The structure of the tri-capacitive-like metallic metasurface proposed in this paper is shown in Fig. 1(a). The metasurface consists of the metal Au and the substrate *SiO*2. The unit cell of metasurface is shown in Fig. 1(b), where Px = 460 nm, Py = 760 nm, a = 250 nm, b = 100 nm, w = 100 nm, $m = l =$ 400 nm, h = 220 nm, g = 50 nm, $\delta 1 =$ 50 nm and $\delta 2 =$ 120 nm. In the simulation, we use the finite difference time domain (FDTD) to study the spectral response of the metasurface. The plane wave is vertically incident, the electric field is polarized along the Y direction and the unit cell is set up with periodic boundary conditions to simulate the infinite array of metasurfaces whose transmission spectra are shown in Fig. 1(c), where g = 100 nm, $\delta 1 = \delta 2 =$ 50 nm (1), g = $\delta 1 = \delta 2 =$ 50 nm (2) and g = $\delta 1 =$ 50 nm, $\delta 2 =$ 120 nm (3). Firstly, keeping the gaps between the left and right sides of the metasurface structure equal, the spectral response corresponds to the top of Fig. 1(c) when g = 100 nm, and the transmittance is the lowest at 176 THz. Then, keeping continuously the gap between the left and right sides of the metasurface equal and reducing the length of the middle gap to 50 nm, the transmittance decreases significantly at 235 THz and the accidental quasi-BIC is excited, which is recorded as BICI. Finally, keeping the left gap unchanged and the middle gap still remain 50 nm, the right gap is increased to 120 nm and the whole metasurface structure is no longer

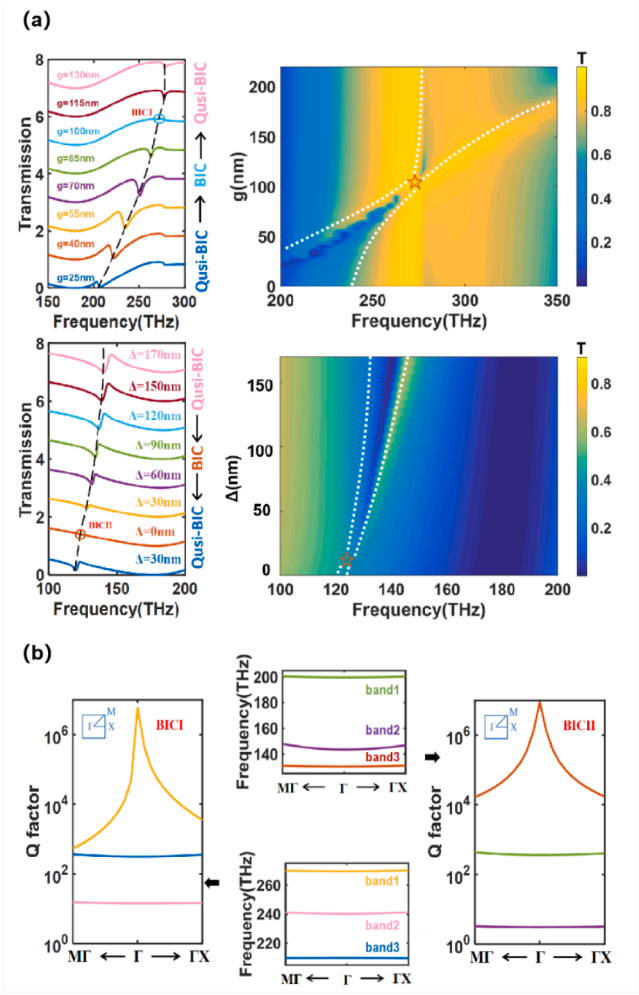

Fig. 2. Parameter sweep for the metasurface in the vicinity of the frequency of BICI and BICII respectively. (a) Discrete spectra and color plot of simulated transmission spectra with different g (Top) and Δ(bottom). For the BICI, fixing the $\delta 1 = \delta 2 = 50$ nm and sweeping g from 0 nm to 220 nm. For the BICII, fixing the g = 50 nm and changing Δ from 0 nm to 170 nm. (b) The corresponding Q factor and band structure for the BICI and BICII.

symmetrical. A clear transmission valley can be observed in the transmission spectrum at 135 THz and the symmetry-protected quasi-BIC is excited, which is recorded as BICII. In this case, BICI is also shifted to a higher frequency, shifting to 243 THz. The corresponding capacitor–inductor model of the metasurface is shown in Fig. 1(d). The three gaps correspond to the three capacitors, and the metals on the top and bottom sides correspond to the inductors. The accidental BIC is formed by the coupling of two modes, dipole mode and LC mode respectively. For BICI, when g = 100 nm, the resonance mode is dipole mode, which has a higher Q value (discussed later), the current direction at the surface of the metamaterial is same, and the electromagnetic wave is released. When g = 50 nm, the resonance mode changes from dipole mode to dipole mode and LC mode coexist, the current direction is opposite at the resonance frequency, and the electromagnetic wave is stored, as shown in Fig. 1(e). Similarly, for BICII, when the structure remains symmetric, the resonance mode of metasurface is dipole mode at 135 THz with the same current direction and released electromagnetic wave, as shown in Fig. 1(f). While in structure (3), the resonance mode is LC mode and dipole mode coexist, the current direction is opposite at the resonance frequency, and the electromagnetic wave is stored. Therefore, by changing the structural parameters of the metasurface, multiple high-Q resonances can be excited in the spectral

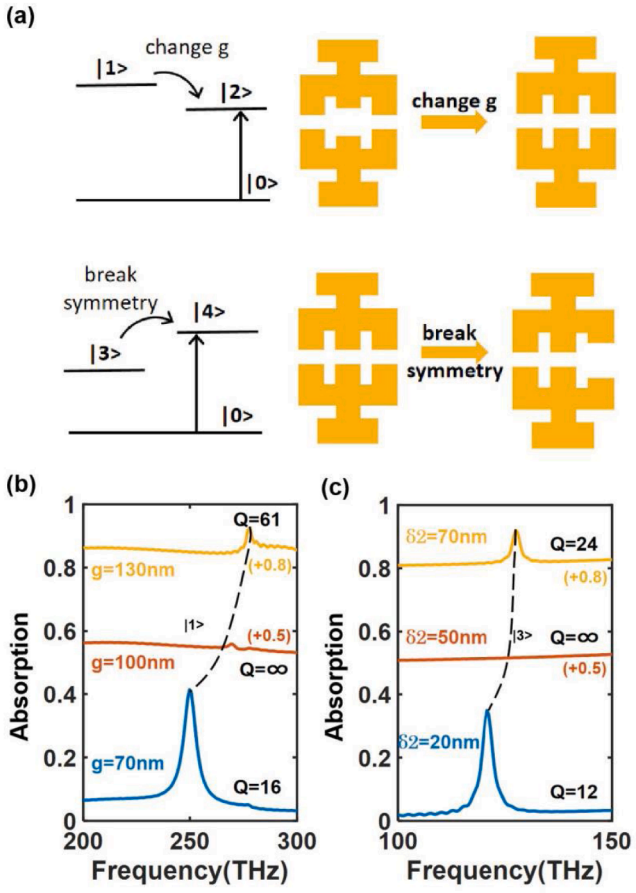

Fig. 3. (a) The level scheme of five-level system for proposed metasurface. (b) and (c) show the corresponding absorption spectra and Q value with different structural parameters for BICI and BICII respectively. The red and yellow lines are obtained by increasing the original values by 0.5 and 0.8, respectively.

response, and the storage and release of electromagnetic waves can be realized.

3. Results and discussions

In the previous part we discussed modal coupling to form accidental BICs and symmetry-protected BICs, and explored the current distribution in different modes to enable the storage and release of electromagnetic waves. In the following section we will explain in detail the process of modal coupling in meta-surface systems. For the accidental BIC, the whole structure remains symmetrical, fixing the left and right gaps unchanged, and the amplitude of the resonance can be changed by adjusting the length of the middle gap. The system with two modes that are coupled with two ports can be explained by temporal couple mode theory, and the dynamics equation of its resonance amplitude can be expressed as [49–52]:

$$\frac{da}{dt} = (j\Omega - \Gamma)a + M^T|s_+\rangle \tag{1}$$

$$|s_-\rangle = C|s_+\rangle + Na \tag{2}$$

where

$$\Omega = \begin{bmatrix} \omega_1 & k \\ k & \omega_2 \end{bmatrix}, \Gamma = \begin{bmatrix} \gamma_1 & \gamma_0 \\ \gamma_0^* & \gamma_2 \end{bmatrix}, C = \begin{bmatrix} r_d & t_d \\ t_d & r_d \end{bmatrix}, N = \begin{bmatrix} n_{11} & n_{12} \\ n_{21} & n_{22} \end{bmatrix} \tag{3}$$

and

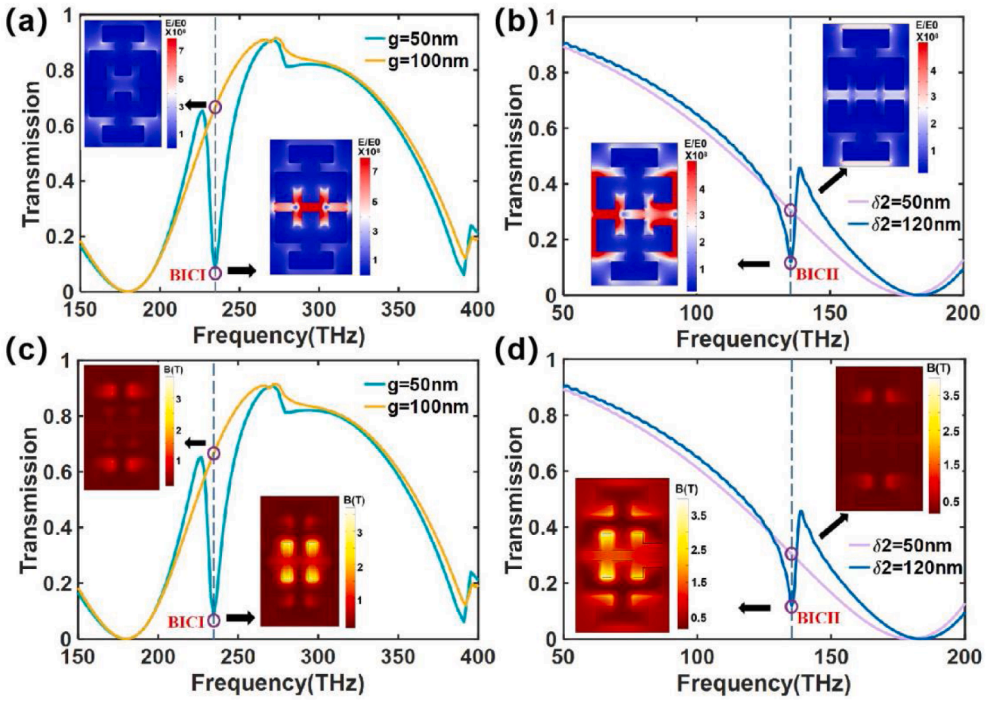

Fig. 4. The local field distribution of BICI and BICII. (a) and (c) represent the electric field and magnetic field enhancement from ideal BIC to quasi-BIC for BICI. (b) and (d) show the electric field and magnetic field enhancement from ideal BIC to quasi-BIC for BICII.

$$|n_{11}| = |n_{21}| = \sqrt{\gamma_1}, |n_{21}| = |n_{22}| = \sqrt{\gamma_2} \tag{4}$$

where a is the resonance amplitude of the mode supported by the system, $\omega 1$ and $\omega 2$ are the resonance frequencies of the two modes, γ_1 and γ_2 are the corresponding decay rates, $\gamma_0{}^*$ and γ_0 is the coupling coefficient generated by the damping, C represents the direct coupling between the input and output ports, M and N represent the coupling between the output and input ports and the modes respectively, and in this system $M = N$. $|s+>$ is the input wave amplitude and $|s->$ is the outgoing wave amplitudes from ports 1 and 2, respectively. Bringing formula (3)–(6) into Eq. (1)–(2) gives:

$$\frac{d}{dt}\begin{bmatrix} a_1 \\ a_2 \end{bmatrix} = (j\Omega - \Gamma)\begin{bmatrix} a_1 \\ a_2 \end{bmatrix} + M\begin{bmatrix} s_{1+} \\ s_{2+} \end{bmatrix} = j\begin{bmatrix} \omega_1 + j\gamma_1 & k + j\gamma_0 \\ k + j\gamma_0^* & \omega_2 + j\gamma_2 \end{bmatrix}\begin{bmatrix} a_1 \\ a_2 \end{bmatrix} + \begin{bmatrix} n_{11} & n_{21} \\ n_{12} & n_{22} \end{bmatrix}\begin{bmatrix} s_{1+} \\ s_{2+} \end{bmatrix} \tag{5}$$

$$\begin{bmatrix} s_{1-} \\ s_{2-} \end{bmatrix} = \begin{bmatrix} r_d & t_d \\ t_d & r_d \end{bmatrix}\begin{bmatrix} s_{1+} \\ s_{2+} \end{bmatrix} + \begin{bmatrix} n_{11} & n_{12} \\ n_{21} & n_{22} \end{bmatrix}\begin{bmatrix} a_1 \\ a_2 \end{bmatrix} \tag{6}$$

The Hamiltonian of this coupled system is defined as:

$$H = j\Omega - \Gamma = j\begin{bmatrix} \omega_1 + j\gamma_1 & k + j\gamma_0 \\ k + j\gamma_0^* & \omega_2 + j\gamma_2 \end{bmatrix} \tag{7}$$

where k is the direct coupling coefficient between the two modes. By adjusting the value of g, when the Friedrich–Wintgen condition is satisfied.

$$k(\gamma_1 - \gamma_2) = \sqrt{\gamma_1\gamma_2}(\omega_1 - \omega_2) \tag{8}$$

An eigenfrequency will become purely real with the decay rate of 0. This means that this eigenmode transforms into the prefect BIC with an infinite Q value ($Q = \omega/2\,\gamma$), which manifests itself in the spectrum as vanishing linewidth, as shown in Fig. 2(a). This metasurface system is symmetrical, so this BIC is called the accidental BIC. The accidental BIC is obtained by the mutual coupling of two low Q mode resonances, and the dipole mode and LC mode are coupled to each other to excite BICI. The resonance frequencies of the two modes remain close to each other, the transmission linewidth disappears in the spectrum and the Q value tends to infinity when parameter g increases from 25 nm to 100 nm until the Friedrich–Wintgen condition is satisfied. As the parameter g continually increases, the resonance frequencies of the two modes continue to shift, the Friedrich–Wintgen condition is not satisfied, the transmission valley can be observed in the spectrum, and the Q value shifts to a finite value. For the symmetry-protected BICs, fixing The Hamiltonian of this coupled system is defined as the middle gap g = 50 nm to remain constant and adjusting the right gap so that the left and right gaps are unequal, thus the symmetry of this unit cell of metasurface structure is broken. We assigned $\Delta = |\delta 1 - \delta 2|$ and the whole structure is symmetric where k is the direct coupling coefficient between the two modes. By adjusting the value of g, when the Friedrich–Wintgen condition is satisfied, an eigenfrequency will become purely real with the decay rate of 0. This means that this eigenmode transforms into the prefect BIC with an infinite Q value ($Q = \omega/2\,\gamma$), which manifests itself in the spectrum as vanishing linewidth, as shown in and forms the symmetry-protected BIC when $\Delta = 0$, whose Q tends to infinity and presents as a vanishing linewidth in the spectrum. With the increase or decrease of δ 2, the symmetry is broken and the BIC couples with the extended states in the continuum each other and leaks into the vacuum. According to the perturbation theory, the symmetry-protected BIC transforms into a quasi-BIC, which Q value becomes finite and a distinct linewidth can be observed in the spectrum. Moreover, its linewidth and resonance amplitude increase with increasing Δ. Furthermore, it has been found that the frequency and amplitude of BICI and BICII are related to the intermediate gap width g and the structural asymmetry Δ respectively by comparison, which gives a large degree of freedom to modulate the two resonances separately.

In order to better describe the formation process of multiple resonances in the system, which contains a ground state, two prefect BICs and two quasi-BICs, a five level system is proposed as shown in Fig. 3(a). In this five level system, $|0>$ is the ground state, and the accidental BICI$|1>$ is realized when the structure remains symmetric and g = 100 nm, which has no interaction with the ground state and its absorption

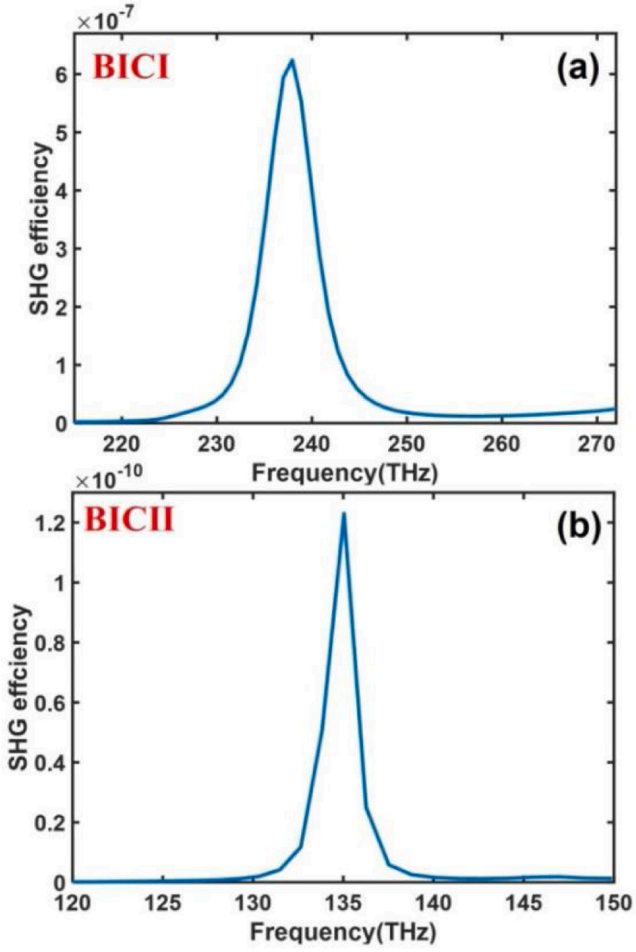

Fig. 5. The simulation calculates the second harmonic generation efficiency at (a) BICI and (b) BICII with the same structural parameters as structure (2) and (3) in Fig. 1(c).

close to 0. Because there is no mutual coupling with the extended states in the continuum, the electromagnetic wave cannot leak into the vacuum and the Q value tends to infinity. Changing the parameter value of g, the accidental BIC transforms into a quasi-BIC |2> with enhanced absorption, mutual coupling with the output port, electromagnetic wave leaks into the vacuum, and the Q value decreases and becomes finite, as shown in Fig. 3(b). It is noted that a little absorption peak can be observed on the right side of the perfect BIC in Fig. 3(b), which is formed by the polarization resonance of the plasmon excitation, independent of the modes coupling, and this small resonance is always present in the absorption spectrum that is not affected by the change of the structural parameters. Assigning the middle gap length g = 50 nm when the left and right gaps are equal, no obvious resonance is observed in the 100–150 THz, which is manifested as symmetry-protected BICII |3> and its Q value tends to infinity. Changing $\delta 2$, the symmetry of the structure is broken and the symmetry-protected BIC transforms into quasi-BIC |4>, whose mutual coupling with the output port can increase the absorption, obvious resonance is observed in the spectrum and Q value decreases and becomes finite. For the ideal BIC, the Q factor should theoretically approach infinity. However, the inherent losses in the metallic metasurface cause the Q value to become finite, corresponding to the simulation results in Fig. 2(b), where the inherent losses are mainly ohmic losses in the metal and dielectric losses in the substrate. In this case, the energy loss from the system to the ports is 0.

In addition to the storage and release of electromagnetic waves and multi-channel resonance, the proposed metasurface structure in this paper also can achieve large local electric field enhancement and magnetic field enhancement due to its support of high Q resonance, the simulation results of which are shown in Fig. 4. For the BICI, the electric field is bound in the intermediate gap and the local field is significantly enhanced when g = 50 nm. Compared to the initial electric field $E0$, the electric field intensity increases about 8×10^8 times. When g increases to 100 nm, the quasi-BIC transforms into the prefect BIC, and the local field enhancement is significantly weakened, which is the result of the input wave not couples with the hybridized modes in the metasurface structure and the disappearance of the resonance linewidth. At the same time, the local magnetic field is also significantly enhanced by shifting g from 100 nm to 50 nm. Compared with the prefect BIC, the magnetic field of the quasi-BIC is enhanced by about 3.7 T, and its distribution is shown in Fig. 4(a) and (c). For BICII, the unit cell of the metasurface constitutes the symmetry-protected BIC and its local field distribution is weak when $\delta 2 = 50$ nm. Increasing $\delta 2$ to 120 nm breaks the symmetry of the structure, and its local electric field is significantly enhanced in the left and right gaps about 5×10^8 times compared to the initial field strength $E0$, while its local magnetic field is also enhanced to some extent inside the metasurface structure compared to the symmetry-protected BIC. The magnetic field strength of the quasi-BIC is enhanced by about 4 T and its distribution is shown in Fig. 4(b) and (d).

The main study of nonlinear optics is the interaction between photons under the irradiation of a high intensity light source. When light strikes the material, the electrons are displaced, producing a scattering field that oscillates synchronously and interferes with the incident light [53]. If the amplitude of the incident light is large enough, the binding of electrons in the material becomes increasingly asymmetric and the bound electron orbitals are distorted. In this case, the optical response of the material is related to the intensity of the incident field. The electron orbital distortion and the resulting optical response can be described by the polarization vector P with both linear and nonlinear terms:

$$P = \varepsilon_0 \chi^{(1)} \cdot E + \varepsilon_0 \chi^{(2)} : EE + \varepsilon_0 \chi^{(3)} \vdots EEE + \cdots \tag{9}$$

where E is the local field, $\varepsilon 0$ is the vacuum dielectric constant, $\chi^{(1)}$ is the linear polarization coefficient, and $\chi^{(2)}$ and $\chi^{(3)}$ are the second- and third-order nonlinear polarization coefficients, respectively. For the second-order nonlinear optical process, the SHG efficiency can be calculated by the following equation:

$$\eta = \frac{I_2(L)}{I_1(0)} = \frac{8\omega^2 d^2 L^2}{\varepsilon_0 n_{2\omega} n_\omega^2 c^3} \frac{P_1(0)}{S} sinc^2\left(\frac{\Delta kL}{2}\right) \tag{10}$$

where ω is the fundamental frequency, d is the octave factor to replace the polarization rate ($d = \chi^{(2)}/2$), L is the thickness of the unit structure, ε is the material dielectric constant of metasurface, c is the speed of light, I_2 is the output octave light intensity, I_1 is the input fundamental frequency light intensity, S is the cross-sectional area of the beam, where $|E1|^2 = P_1/S$, $E1$ is the fundamental frequency light field intensity, P_1 is the input optical power at fundamental frequency, Δk is the phase mismatch factor, and $\Delta k = 0$ if the phase is matched. According to the above equation, the SHG efficiency depends on the electric field strength of the fundamental frequency light. In addition, the nonlinear efficiency usually rises and falls in the ratio of $(Q/V)^n$, where Q is the quality factor of the considered resonance, V is the cavity volume, and n is the nonlinear order. The nonlinear optical efficiency can be increased by 10^3-10^5 as the subwavelength metasurface cavity volume decreases and the resonant Q value increases. From the previous simulation results, it can be seen that the metasurface structure designed in this paper can excite two high-Q resonances and significantly enhance the electric field intensity at the resonant frequency by two parameter adjustments. The study has calculated the SHG efficiency of the metasurface and the results are shown in Fig. 5. At the resonant frequencies corresponding to BICI and BICII, the second-order nonlinear efficiency is significantly enhanced, reaching 6×10^{-7} and 1.2×10^{-10}, respectively. The difference in nonlinear efficiency at the resonance of the two quasi-BICs is

related to the intensity of the local field. According to previous simulations, the local field strength of the Friedrich–Wintgen quasi-BIC excited by adjusting the middle spacing is higher than that of the symmetry-protected quasi-BIC excited by breaking the symmetry.

4. Conclusion

In this paper, the designed tri-capacitance-like metasurface structure excites the Friedrich–Wintgen quasi-BIC and the symmetry-protected quasi-BIC by adjusting the structure parameters step-by-step to achieve two-channel high-Q resonance and local field enhancement, and the second harmonic efficiency is enhanced at both resonant frequencies. The simulation results show that the nonlinear efficiency at the Friedrich–Wintgen quasi-BIC is about 10^3 times higher than that of the symmetry-protected quasi-BIC, which is related to the enhancement of the local field. Moreover, the current distribution is different at the resonant frequency corresponding to different structural parameters. The in-phase current direction corresponds to the release of electromagnetic waves and the opposite-phase current direction corresponds to the storage of electromagnetic waves. The proposed metasurface in this research would be applied in nonlinear optics, multi-channel communication, and fast communication where electromagnetic wave storage and release are required.

Declaration of competing interest

The authors declare that they have no known competing financial interests or personal relationships that could have appeared to influence the work reported in this paper.

Data availability

Data will be made available on request.

Funding

This work was financially sponsored by Open Fund of State Key Laboratory of Millimeter Wave, Southeast University (K202216) and National Natural Science Foundation of China (12104339, 52227814).

References

[1] Q.A. Cheng, W.X. Jiang, T.J. Cui, Radiation of planar electromagnetic waves by a line source in anisotropic metamaterials, J. Phys. D: Appl. Phys. 43 (2010) 6.
[2] Yijun Feng, Qi Hu, Kai Qu, et al., Reconfigurable intelligent surfaces: design, implementation, and practical demonstration, Electromagn. Sci. 1 (2) (2023), 0020111, https://doi.org/10.23919/emsci.2022.0011.
[3] J.B. Pendry, Negative refraction makes a perfect lens, Phys. Rev. Lett. 85 (2000) 3966–3969.
[4] Z.Y. Zhang, S. Liang, F. Li, S.H. Ning, Y.M. Li, G. Malpuech, Y.P. Zhang, M. Xiao, D. Solnyshkov, Spin–orbit coupling in photonic graphene, Optica 7 (2020) 455–462.
[5] X. Xiong, Y.F. Chen, H. Wang, S.Q. Hu, Y.H. Luo, J.L. Dong, W.G. Zhu, W.T. Qiu, H. Y. Guan, H.H. Lu, J.H. Yu, J. Zhang, Z. Chen, Plasmonic interface modified with graphene oxide sheets overlayer for sensitivity enhancement, ACS Appl. Mater. Interfaces 10 (2018) 34916–34923.
[6] R. Ge, J.L. Xie, B. Yan, E.X. Liu, W. Tan, J.J. Liu, Refractive index sensor with high sensitivity based on circular photonic crystal, J. Opt. Soc. Amer. 35 (2018) 992–997.
[7] J.W. You, Q. Ma, L. Zhang, C. Liu, J. Zhang, S. Liu, T.J. Cui, Electromagnetic metamaterials: From classical to quantum, Electromagn. Sci. 1 (1) (2023) 1–33.
[8] J.W. You, Z. Lan, Q. Ma, Z. Gao, Y. Yang, F. Gao, M. Xiao, T.J. Cui, Topological metasurface: From passive toward active and beyond, Photonics Res. 11 (3) (2023) B65–B102.
[9] X.T. Lai, Q. Ren, F. Vogelbacher, W.E.I. Sha, X.Y. Hou, X. Yao, Y.L. Song, M.Z. Li, Bioinspired quasi-3D multiplexed anti-counterfeit imaging via self-assembled and nanoimprinted photonic architectures, Adv. Mater. 34 (2022) 10.
[10] N. Liu, M. Mesch, T. Weiss, M. Hentschel, H. Giessen, Infrared perfect absorber and its application as plasmonic sensor, Nano Lett. 10 (2010) 2342–2348.
[11] S. Chen, Q. Ren, K. Zhang, W.E.I. Sha, T.T. Hao, H.B. Xu, J.P. Zhao, Y. Li, A highly sensitive and flexible photonic crystal oxygen sensor, Sensors Actuators B 355 (2022) 9.
[12] H.Q. Zhou, Y.T. Wang, X.W. Li, Q. Wang, Q.S. Wei, G.Z. Geng, L.L. Huang, Switchable active phase modulation and holography encryption based on hybrid metasurfaces, Nanophotonics 9 (2020) 905–912.
[13] S.L. Sun, Q. He, J.M. Hao, S.Y. Xiao, L. Zhou, Electromagnetic metasurfaces: physics and applications, Adv. Opt. Photonics 11 (2019) 380–479.
[14] D.D. Wen, F.Y. Yue, W.W. Liu, S.Q. Chen, X.Z. Chen, Geometric metasurfaces for ultrathin optical devices, Adv. Opt. Mater. 6 (2018) 17.
[15] W.W. Liu, Z.C. Li, H. Cheng, S.Q. Chen, J.G. Tian, Momentum analysis for metasurfaces, Phys. Rev. A 8 (2017) 10.
[16] N.F. Yu, P. Genevet, M.A. Kats, F. Aieta, J.P. Tetienne, F. Capasso, Z. Gaburro, Light propagation with phase discontinuities: Generalized laws of reflection and refraction, Science 334 (2011) 333–337.
[17] Z.C. Li, W.W. Liu, H. Cheng, S.Q. Chen, J.G. Tian, Manipulation of the photonic spin hall effect with high efficiency in gold-nanorod-based metasurfaces, Adv. Opt. Mater. 5 (2017) 8.
[18] G. Li, S. Chen, N. Pholchai, B. Reineke, P.W. Wong, E.Y. Pun, K.W. Cheah, T. Zentgraf, S. Zhang, Continuous control of the nonlinearity phase for harmonic generations, Nature Mater. 14 (2015) 607–612.
[19] M. Fang, N.H. Shen, W.E.I. Sha, Z.X. Huang, T. Koschny, C.M. Soukoulis, Nonlinearity in the dark: Broadband terahertz generation with extremely high efficiency, Phys. Rev. Lett. 122 (2019) 6.
[20] L. Carletti, A. Locatelli, O. Stepanenko, G. Leo, C. De Angelis, Enhanced second-harmonic generation from magnetic resonance in AlGaAs nanoantennas, Opt. Express 23 (2015) 26544–26550.
[21] Z. Li, W.W. Liu, G.Z. Geng, Z.C. Li, J.J. Li, H. Cheng, S.Q. Chen, J.G. Tian, Multiplexed nondiffracting nonlinear metasurfaces, Adv. Funct. Mater. 30 (2020) 12.
[22] H.Y. Deng, C.M. Huang, Y.J. He, F.W. Ye, Quantum plasmon enhanced nonlinear wave mixing in graphene nanoflakes, Chin. Phys. B 30 (2021) 9.
[23] Q. Ren, J.W. You, N.C. Panoiu, Large enhancement of the effective second-order nonlinearity in graphene metasurfaces, Phys. Rev. B 99 (2019) 10.
[24] J.W. You, Z. Lan, N.C. Panoiu, Four-wave mixing of topological edge plasmons in graphene metasurfaces, Sci. Adv. 6 (13) (2020) eaaz3910.
[25] C.W. Hsu, B. Zhen, A.D. Stone, J.D. Joannopoulos, M. Soljacic, Bound states in the continuum, Nat. Rev. Mater. 1 (2016) 13.
[26] Z. Liu, Y. Xu, Y. Lin, J. Xiang, T. Feng, Q. Cao, J. Li, S. Lan, J. Liu, High-Q quasibound states in the continuum for nonlinear metasurfaces, Phys. Rev. Lett. 123 (2019), 253901.
[27] Z.F. Sadrieva, M.A. Belyakov, M.A. Balezin, P.V. Kapitanova, E.A. Nenasheva, A. F. Sadreev, A.A. Bogdanov, Experimental observation of a symmetry-protected bound state in the continuum in a chain of dielectric disks, Phys. Rev. A 99 (2019) 10.
[28] Q. Ren, F. Feng, X. Yao, Q. Xu, M. Xin, Z. Lan, J. You, X. Xiao, W.E.I. Sha, Multiplexing-oriented plasmon-MoS2 hybrid metasurfaces driven by nonlinear quasi bound states in the continuum, Opt. Express 29 (2021) 5384–5396.
[29] X. Wang, J. Xin, Q. Ren, H. Cai, J. Han, C. Tian, P. Zhang, L. Jiang, Z. Lan, J. You, W.E.I. Sha, Plasmon hybridization induced by quasi bound state in the continuum of graphene metasurfaces oriented for high-accuracy polarization-insensitive two-dimensional sensors, Chin. Opt. Lett. 20 (2022).
[30] T. Shi, Z. Deng, G. Geng, X. Zeng, Y. Zeng, H. Guangwei, A. Overvig, J. Li, C. Qiu, A. Alù, Y. Kivshar, X. Li, Planar chiral metasurfaces with maximal and tunable chiroptical response driven by bound states in the continuum, Nature Commun. 13 (2022) 4111.
[31] L.Q. Cong, R. Singh, Symmetry-protected dual bound states in the continuum in metamaterials, Adv. Opt. Mater. 7 (2019) 7.
[32] H. Friedrich, D. Wintgen, Interfering resonances and bound states in the continuum, Phys. Rev. A 32 (1985) 3231–3242.
[33] S. Han, P. Pitchappa, W. Wang, Y.K. Srivastava, M.V. Rybin, R. Singh, Extended bound states in the continuum with symmetry-broken terahertz dielectric metasurfaces, Adv. Opt. Mater. 9 (2021).
[34] Y. Liang, C. Peng, K. Sakai, S. Iwahashi, S. Noda, Three-dimensional coupled-wave model for square-lattice photonic crystal lasers with transverse electric polarization: A general approach, Phys. Rev. B 84 (2011), 195119.
[35] J.M. Foley, S.M. Young, J.D. Phillips, Symmetry-protected mode coupling near normal incidence for narrow-band transmission filtering in a dielectric grating, Phys. Rev. B 89 (2014) 9.
[36] S. Romano, G. Zito, S. Torino, G. Calafiore, E. Penzo, G. Coppola, S. Cabrini, I. Rendina, V. Mocella, Label-free sensing of ultralow-weight molecules with all-dielectric metasurfaces supporting bound states in the continuum, Photonics Res. 6 (2018) 726–733.
[37] Y. Zhou, H. Zheng, I.I. Kravchenko, J. Valentine, Flat optics for image differentiation, Nat. Photonics 14 (2020) 316–323.
[38] A. Tittl, A. Leitis, M.K. Liu, F. Yesilkoy, D.Y. Choi, D.N. Neshev, Y.S. Kivshar, H. Altug, Imaging-based molecular barcoding with pixelated dielectric metasurfaces, Science 360 (2018) 1105.
[39] K. Koshelev, A. Bogdanov, Y. Kivshar, Meta-optics and bound states in the continuum, Sci. Bull. 64 (2019) 836–842.
[40] A. Kodigala, T. Lepetit, Q. Gu, B. Bahari, Y. Fainman, B. Kante, Lasing action from photonic bound states in continuum, Nature 541 (2017) 196–199.
[41] Y. Lu, X. Feng, Q. Wang, X. Zhang, M. Fang, W.E.I. Sha, Z. Huang, Q. Xu, L. Niu, X. Chen, C. Ouyang, Y. Yang, X. Zhang, E. Plum, S. Zhang, J. Han, W. Zhang, Integrated terahertz generator-manipulators using epsilon-near-zero-hybrid nonlinear metasurfaces, Nano Lett. 21 (2021) 7699–7707.
[42] Y. Zhao, Y. Yang, H.B. Sun, Nonlinear meta-optics towards applications, PhotoniX 2 (2021) 3, https://doi.org/10.1186/s43074-021-00025-1.

[43] T. Nakanishi, T. Otani, Y. Tamayama, M. Kitano, Storage of electromagnetic waves in a metamaterial that mimics electromagnetically induced transparency, Phys. Rev. B 87 (2013), 161110.
[44] L. Xu, K.Z. Kamali, L. Huang, M. Rahmani, A. Smirnov, R.C. Morales, Y. Ma, G. Zhang, M. Woolley, D. Neshev, A.E. Miroshnichenko, Dynamic nonlinear image tuning through magnetic dipole quasi-BIC ultrathin resonators, Adv. Science 6 (2019), 1802119.
[45] I. Volkovskaya, L. Xu, L. Huang, A.I. Smirnov, A.E. Miroshnichenko, D. Smirnova, Multipolar second- harmonic generation from high-Q quasi-BIC states in subwavelength resonators, Nanophotonics 9 (2019) 3953–3963.
[46] L. Huang, L. Xu, M. Rahmani, D. Neshev, A.E. Miroshnichenko, Pushing the limit of high-Q mode of a single dielectric nanocavity, Adv. Photonics 3 (2021), 016004–016004.
[47] Y. Yu, Y. Yu, L. Huang, H. Peng, L. Xiong, L. Cao, Giant gating tunability of optical refractive index in transition metal dichalcogenide monolayers, Nano Letters 17 (2017) 3613–3618.
[48] L. Huang, Y. Yu, L. Cao, General modal properties of optical resonances in subwavelength nonspherical dielectric structures, Nano Letters 13, 3559–3565.
[49] R. Kikkawa, M. Nishida, Y. Kadoya, Polarization-based branch selection of bound states in the continuum in dielectric waveguide modes anti-crossed by a metal grating, New J. Phys. 21 (2019) 11.
[50] A. Volya, V. Zelevinsky, Non-Hermitian effective Hamiltonian and continuum shell model, Phys. Rev. C 67 (2003), 054322.
[51] J. Li, Z. Yue, J. Li, C. Zheng, Y. Zhang, J. Yao, Ultra-narrowband terahertz circular dichroism driven by planar metasurface supporting chiral quasi bound states in continuum, Opt. Laser Technol. 161 (2023), 109173.
[52] X. Zheng, J. Lin, Z. Wang, et al., Manipulating light transmission and absorption via an achromatic reflectionless metasurface, PhotoniX 4 (2023) 3, https://doi.org/10.1186/s43074-022-00078-w.
[53] J. Hou, J. Lin, J. Zhu, et al., Self-induced transparency in a perfectly absorbing chiral second-harmonic generator, PhotoniX 3 (2022) 22, https://doi.org/10.1186/s43074-022-00068-y.